Theoretical Studies on the Reaction Kinetic of 2-Acetylfuran with Hydroxyl Radicals

Wei He, Kaixuan Chen, Liucun Zhu,* and Kang Shen*

Read Online

ACCESS | Metrics & More | Article Recommendations

ABSTRACT: With the development of synthetic methods, 2-acetylfuran (AF2) has become a potential biomass fuel. The potential energy surfaces of AF2 and OH including OH-addition reactions and H-abstraction reactions were constructed by theoretical calculations at the CCSDT/CBS/M06-2x/cc-pVTZ level. The temperature- and pressure-dependent rate constants of the relevant reaction pathways were solved based on transition state theory and Rice−Ramsperger−Kassel−Marcus theory, as well as Eckart tunneling effect correction. The results showed that the H-abstraction reaction on CH_3 on the branched chain and the OH-addition reaction at the C (2) and C (5) sites on the furan ring were the main reaction channels in the reaction system. At low temperatures, the AF2 and OH-addition reactions dominate, and the percentage decreases gradually to zero with increasing temperature, and at high temperatures, the H-abstraction reactions on the branched chains become the most dominant reaction channel. The rate coefficients calculated in the current work improve the combustion mechanism of AF2 and provide theoretical guidance for the practical application of AF2.
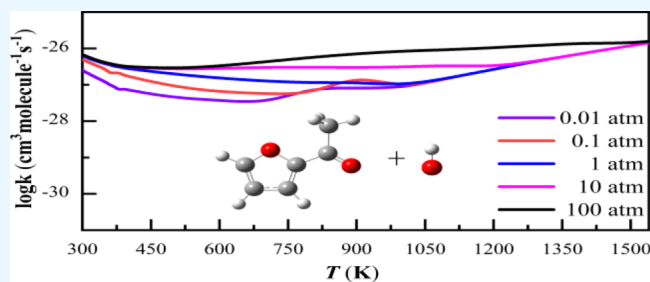
1. INTRODUCTION

Considering the strict emission regulations of the automobile industry and the increasing global energy demand and price, people are vigorously researching and developing renewable energy to replace fossil derivative products in an economically and environmentally sustainable way to meet the future demand.[1−4] Biofuels, liquid, or gas fuels derived from biomass are considered the natural successors to petroleum derived products that dominate the transportation industry because they have many desirable fuel characteristics.[5−8]

Recently, some new methods have been proposed to produce alkylfuran in large quantities from lignocellulosic biomass and even non-edible biomass.[9−12] Furan and its derivatives have received much attention because of their suitable physicochemical properties.[13]

Su et al.[14] conducted experiments on the pyrolysis of 3-methylfuran in a flow reactor at low pressure (30 Torr) and atmospheric pressure, identified and measured more than 20 pyrolysis species, developed a pyrolysis model based on the experimentally detected species, and validated the model with experimental results. Whelan et al.[15] calculated the rate constants for the reactions of OH with furans, 2-methylfuran and 2,5-dimethylfuran. The results showed that OH-addition dominates, while H-abstraction reactions become increasingly important when the temperature is above 900 K. Wang et al.[16] investigated the low-temperature oxidation experiments of 2-methylfuran in a jet-stirred reactor (JSR) and showed that the consumption pathway of 2-methylfuran in low-temperature

oxidation consists mainly of OH/H addition and methyl H-abstraction reactions on the branched chain. Jin et al.[17] conducted low-temperature oxidation experiments and laminar burning velocity measurements on furfural and constructed a combustion model for furfural by theoretical calculations, which can predict the experimental results of furfural well. Li et al.[18] carried out the experiments on the low-temperature oxidation of 2-ethylfuran with different equivalence ratios in JSR and improved a detailed low-temperature oxidation kinetic model based on the previous model by theoretical calculations, which can predict the experimental results well.

Researchers have found that the reaction between fuel molecules and small free radicals such as H and OH radicals is essential for predicting various combustion parameters under different pressure and temperature conditions.[19−23] Zhang et al.[19] studied the rate constants of methyl butyrate with H and OH radicals by solving the master equation calculations by transition state theory and compared with experimental data. Zhou et al.[20] constructed the potential energy surface (PES) of the reaction between methyl crotonate and OH by quantum
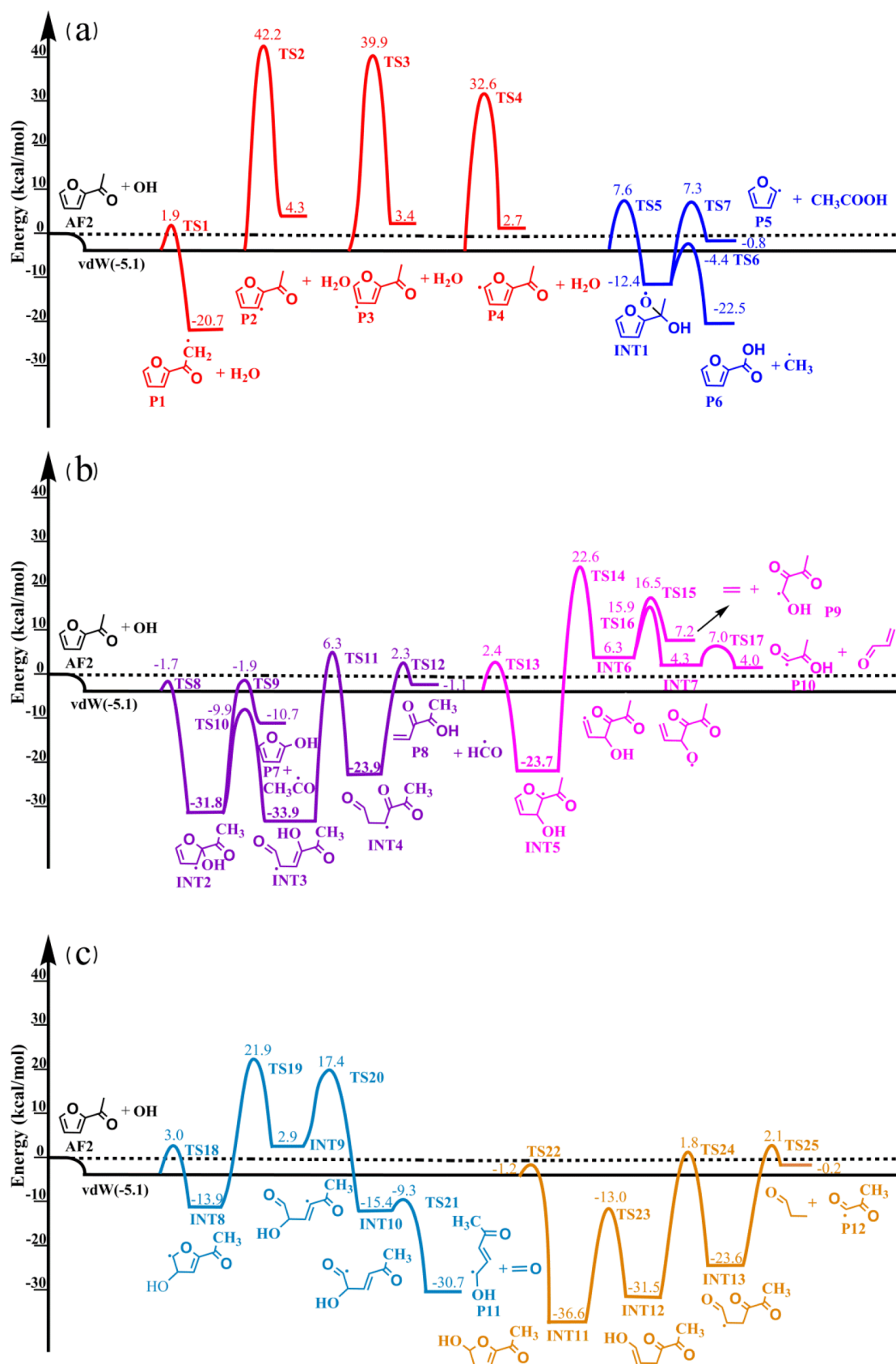
Figure 1. PES for the reaction of AF2 with OH constructed at the CCSDT/CBS/M06-2x/cc-pVTZ level. The energies of the species on the PES are all relative to the energy of AF2 + OH unit in kcal•mol^{-1}. (a) H-abstraction reactions and addition reactions on branched chains; (b) addition reactions at the C (2) and C (3) sites; (c) addition reactions at the C (4) and C (5) sites.

chemistry, calculated the rate constants of the reaction, and updated the combustion model of methyl crotonate, and the updated model reproduced the experimental results well. Jin et al.[21] measured the rate constants of the reactions of OH with cyclopentadiene and indene in the temperature range of 828−1390 K and at a pressure close to 1 atm. The experimental results showed that the reaction of OH with cyclopentadiene was about 2 times faster than that of indene. He et al.[22] constructed the PES of methyl 2-furoate and OH by theoretical calculations, which showed that the H-abstraction on the branched CH_3 and the addition reaction at the C (2) and C (5) on the furan ring were the main consumed channels. Xing et al.[23] calculated the rate constants for the reaction of 2-furoyl alcohol with OH by high-level quantum chemistry and showed that the OH-addition reaction dominates at $T \leq 1300$ K and the H-abstraction reaction rate is faster on the branched chains than on the furan ring.

The main difference between 2-acetylfuran (AF2) and furan and its derivatives is the branched structure. In order to study the influence of the branched structure in the furan fuel molecule on the combustion products of the furan fuel, the reaction of AF2 with OH was studied through theoretical calculations. This study investigated all possible reaction pathways of AF2 with OH by using highly accurate theoretical methods. The rate constants of the reaction channels were computed via the solution of the master equation. This study may improve the understanding of the combustions of the furan series bio-fuel.

2. METHODOLOGY

Structural optimization and frequency calculation of the stationary and saddle points on the PES were performed at the M06-2X/cc-pVTZ level.[24] The transition state structure is identified with one and only one imaginary frequency. A relaxed one-dimensional scan of all stationary points on the PES is performed along the corresponding dihedral angle increments of 10° to find the lowest energy conformation. To obtain more accurate single-point energies, the CCSD(T) method and cc-pVXZ (X = D, T) basis sets were used and obtained by the extrapolation of the basis sets to the complete basis sets.[22] Calculation of the DFT is performed on the Gaussian 09 software package.[25]

The temperature- and pressure-dependent rate constants for the relevant reactions on the PES were calculated based on the transition state theory and the Rice−Ramsperger−Kassel−Marcus theory, as well as the Eckart tunneling effect correction by solving the master equation with the MESS program package.[26,27] The Lennard-Jones model was used to estimate the collision frequency between the dilute gas (argon, Ar) and the reactants with parameters σ = 3.47 Å, ε = 79.20 cm^{-1} and σ = 5.50 Å, ε = 362.53 cm^{-1} for Ar and the reactants, respectively, where the parameters for Ar were obtained from previous studies[28] and the parameters for AF2 and OH were obtained by Joback's group contribution method.[29] The collision energy transfer was calculated by a single exponential down model, $<\Delta E>_{down}$ = 300 × $(T/300)^{0.85}$ cm.[22] The low-frequency torsional mode of the stationary point on the PES corresponding to the internal rotation is treated as a one-dimensional hindered rotor with hindered potential, which is obtained by relaxed scanning in 10° increments at the M06-2X/cc-pVTZ level.
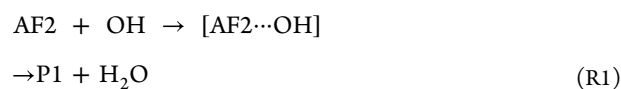
Due to the carbonyl group on the branched acetyl group of AF2 forms a weak van derWaals (vdW) complex with OH via

hydrogen bonding. The reaction transition state of this barrierless reaction is so loose that its rate constant cannot be calculated by conventional transition state theory, so in the current study, the rate constant of this process is calculated by phase space theory.[20] The interaction between the reactants and the weak complex is estimated by the eq $V(R) = C_6/R^6$, where R is the distance between the reactants. C_6 was estimated by the equation $C_6 = \alpha_1 \cdot \alpha_2 \cdot E_1 \cdot E_2/(E_1 + E_2)$, where α_i and $E_i(i = 1, 2)$ are the polarization rate and ionization energy of the two reactants, respectively. The value of C_6 in the current system was calculated at the level of G4 as 3.59 × 10^5 cm^{-1}·Å^6.

3. RESULT AND DISCUSSION

The PESs for the H-abstraction reactions and addition reactions of AF2 with OH were constructed, as shown in Figure 1. In addition, the subsequent decomposition pathway of the intermediate species generated by the addition reaction of the OH with AF2 was constructed.

3.1. Potential Energy Surfaces. *3.1.1. H-Abstraction Reaction.* From Figure 1a, it can be seen that there are four sites of AF2 where H-abstraction from the OH may react, namely, the H on the branched CH_3 and the H atom on the three sites of the furan ring, eventually producing $C_6H_5O_2$ radicals and H_2O.

$$AF2 + OH \rightarrow [AF2\cdots OH]$$

$$\rightarrow P1 + H_2O \qquad (R1)$$

$$\rightarrow P2 + H_2O \qquad (R2)$$

$$\rightarrow P3 + H_2O \qquad (R3)$$

$$\rightarrow P4 + H_2O \qquad (R4)$$

The energy barriers for the four H-abstraction reactions can be seen to be CH_3 < C (5) < C (4) < C (3), with the lowest energy barrier for the H atom on the branched CH_3 to react with the OH and the highest energy barrier for the C (3) site.

He et al.[30] calculated the dissociation energies of AF2 at the CBS-QB3 level, and the results showed that the dissociation energies of the H atoms on the branched CH_3, C (3), C (4), and C (5) were 95.3, 120.4, 119.5, and 118.8 kcal•mol^{-1}, respectively. This similarly suggests that the H atom on the branched CH_3 is the active site for the AF2 H-abstraction reaction. The OH to abstract the H atom on the furan ring needs to overcome a very high energy barrier resulting in a reaction that does not occur easily. Therefore, it can be considered that the reaction between the H atom of the CH_3 on the branched chain of AF2 and the OH is the main reaction channel.

The transition state structures TS1, TS2, TS2, and TS4 at the four sites, where the H-abstraction reaction of AF2 occurs, are illustrated in Figure 2. The transition state structures of TS1, TS2, TS3, and TS4 are for the CH_3, C (3), C (4), and C (5) sites, respectively.

From the structure of TS1, it can be seen that the distance between the O (7) on the carbonyl group and the H (16) on the OH in the branched chain is 2.100 Å. O and H may easily form hydrogen bonds through weak interactions within this distance range.[22] In the TS1 structure, the OH forms a 6-membered ring transition state structure by hydrogen bonds with the H on the CH_3 of the AF2 branched chain and the O atom on the carbonyl group of the AF2 branched chain. The
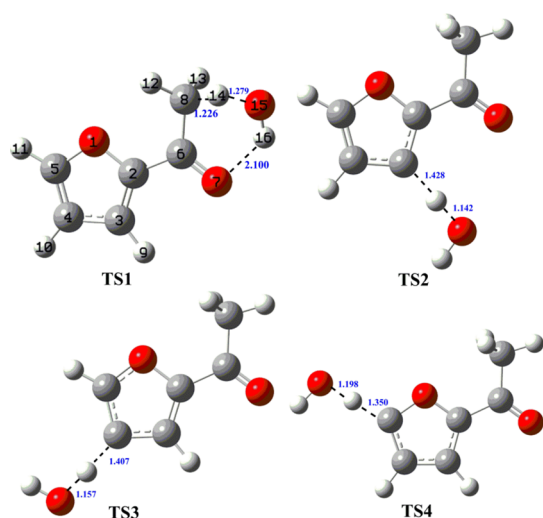
Figure 2. Calculated transition state structures TS1, TS2, TS3, and TS4 for the reaction of AF2 + OH H-abstraction at the level of M06-2x/cc-pVTZ with bond length units of Å.
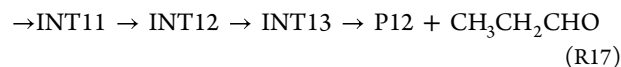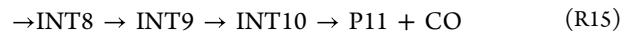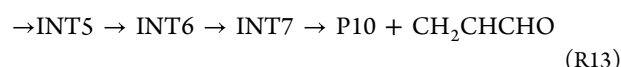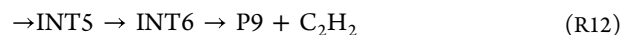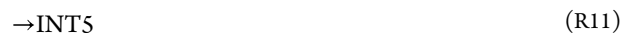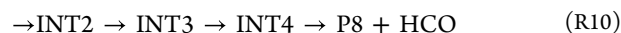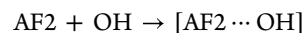
transition state structure of this is very stable and may also be responsible for the lower TS1 energy barrier and potentially increase the branching ratio of this reaction channel.

3.1.2. OH-Addition Reaction. In addition to H-abstraction reactions with AF2, OH may undergo addition reactions to C=C double bonds on furan rings and C=O double bonds of carbonyl groups on branched chains. As shown in Figure 1a−c, the OH undergoes an addition reaction with the carbonyl group on the AF2 branched chain and C(2)−C (5) on the furan ring to generate $C_6H_7O_3$ radicals, namely INT1, INT2, INT5, INT8, and INT11.
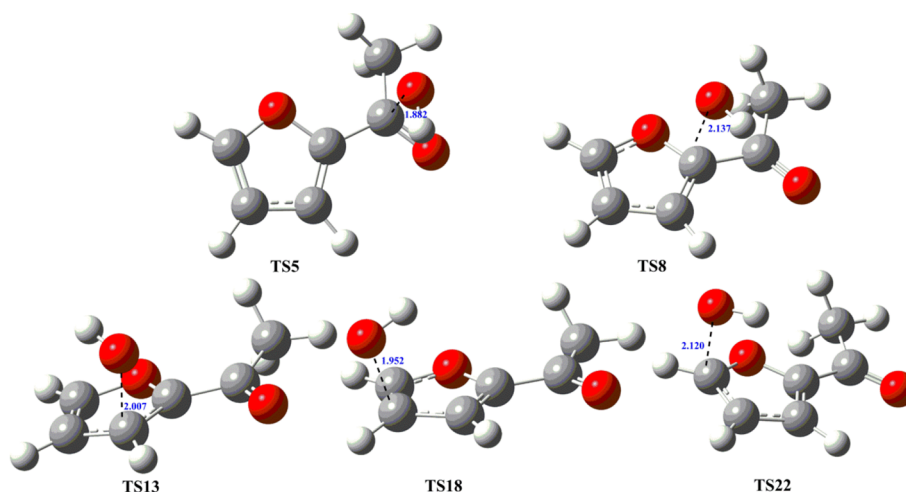
The transition state structures calculated at the M06-2x/cc-pVTZ level for the AF2 and OH addition reactions are shown in Figure 3. TS5, TS8, TS13, TS18, and TS22 are transition state structures with OH addition at the carbonyl, C (2), C (3), C (4), and C (5) sites, respectively. The energy barriers of the transition states TS5, TS8, TS13, TS18, and TS22 for OH addition to AF2 are 7.6, −1.7, 2.4, 3.0 and − 1.2 kcal•mol^{-1}, respectively, as can be seen from Figure 1a−c. OH addition to the C=O double bond on the branched carbonyl of AF2 has a

much higher energy barrier than the C=C double bond on the AF2 ring, so the OH addition reaction on the branched chain is not competitive compared to that on the furan ring. The OH addition energy barrier at C (2) on the AF2 ring is the lowest, followed by site C (5), and the highest energy barrier at C (3). Energetically, C (2) and C (5) are the main OH addition channels.

The PESs of the subsequent decomposition paths of the intermediate species INT1, INT2, INT5, INT8, and INT11 generated by the OH addition to AF2 are also constructed, as seen in Figure 1a−c. In the current study, the subsequent isomerization reactions and β-dissociation reactions of INT1, INT2, INT5, INT8, and INT11 were mainly considered.

$$AF2 + OH \rightarrow [AF2 \cdots OH]$$

$$\rightarrow INT1 \tag{R5}$$

$$\rightarrow INT1 \rightarrow P5 + CH_3COOH \tag{R6}$$

$$\rightarrow INT1 \rightarrow P6 + CH_3 \tag{R7}$$

$$\rightarrow INT2 \tag{R8}$$

$$\rightarrow INT2 \rightarrow P7 + CH_3CO \tag{R9}$$

$$\rightarrow INT2 \rightarrow INT3 \rightarrow INT4 \rightarrow P8 + HCO \tag{R10}$$

$$\rightarrow INT5 \tag{R11}$$

$$\rightarrow INT5 \rightarrow INT6 \rightarrow P9 + C_2H_2 \tag{R12}$$

$$\rightarrow INT5 \rightarrow INT6 \rightarrow INT7 \rightarrow P10 + CH_2CHCHO \tag{R13}$$

$$\rightarrow INT8 \tag{R14}$$

$$\rightarrow INT8 \rightarrow INT9 \rightarrow INT10 \rightarrow P11 + CO \tag{R15}$$

$$\rightarrow INT11 \tag{R16}$$

$$\rightarrow INT11 \rightarrow INT12 \rightarrow INT13 \rightarrow P12 + CH_3CH_2CHO \tag{R17}$$

The AF2 undergoes an addition reaction (R5) with the OH to form INT1, which is subsequently consumed by β-breaking R6 and R7. In reaction R6, INT1 breaks the C−C bond through TS7 to produce 2-furyl radical (P5) + acetic acid (CH$_3$COOH) with an energy barrier of 7.3 kcal•mol^{-1}. Within

Figure 3. Calculated transition state structures TS5, TS8, TS13, TS18, and TS22 for the addition reaction of AF2 + OH at the level of M06-2x/cc-pVTZ with bond length units of Å.

Table 1. Rate Coefficients in Modified Arrhenius Expressions for the AF2 + OH Reaction System, $k = AT^n \exp(-E_a/RT)$

reaction	p (atm)	A (cm^3•mol^{-1}•s^{-1})	n	E_a (cal•mol^{-1})
total	0.01	3.01E−22	3.06	−3.35E+03
	0.1	8.56E−20	2.32	−2.52E+03
	1	2.32E−19	2.19	−2.45E+03
	10	5.10E−17	1.51	−1.55E+03
	100	2.30E−17	1.64	−1.60E+03
AF2 + OH → P1 + H$_2$O		7.78E−22	3.07	−6.59E+02
AF2 + OH → P2 + H$_2$O		8.43E−76	18.45	−8.79E+02
AF2 + OH → P3 + H$_2$O		4.34E−75	18.43	−1.47E+03
AF2 + OH → P4 + H$_2$O		1.96E−65	15.49	−1.36E+03
AF2 + OH → INT1	0.01	7.21E−22	3.45	1.70E+04
	0.1	1.10E−30	3.75	4.84E+03
	1	3.71E−33	3.95	1.76E+02
	10	1.99E−33	4.95	−2.43E+02
	100	5.37E−31	5.15	2.18E+03
AF2 + OH → INT2	0.01	1.78E+05	−6.36	1.84E+03
	0.1	2.40E+01	−4.84	1.51E+03
	1	2.06E−06	−2.36	2.72E+02
	10	6.28E−11	−0.78	−5.48E+02
	100	6.27E−17	1.18	−2.15E+03
AF2 + OH → INT5	0.01	2.23E+06	−6.55	6.05E+03
	0.1	3.36E−01	−4.13	4.91E+03
	1	3.52E−10	−1.03	3.16E+03
	10	3.21E−19	2.05	1.31E+03
	100	8.25E−19	1.94	1.50E+03
AF2 + OH → INT8	0.01	5.22E+16	−10.35	7.87E+03
	0.1	7.33E+05	−6.39	6.28E+03
	1	4.44E−03	−3.45	4.97E+03
	10	2.11E−18	1.88	2.11E+03
	100	3.72E−18	1.79	2.15E+03
AF2 + OH → INT11	0.01	9.32E−06	−2.53	5.53E+02
	0.1	1.02E−13	0.12	−1.43E+03
	1	5.75E−09	−1.31	2.06E+02
	10	1.83E−15	0.89	−1.22E+03
	100	4.51E−16	1.13	−1.25E+03
AF2 + OH → P5 + CH$_3$COOH		1.46E−48	11.42	4.13E+03
AF2 + OH → P6 + CH$_3$		6.23E−21	2.33	5.78E+03
AF2 + OH → P7 + CH$_3$CO		7.79E−53	13.17	−2.74E+03
AF2 + OH → P8 + HCO		2.48E−64	17.07	9.10E+03
AF2 + OH → P9 + C$_2$H$_2$		4.24E−12	0.99	2.69E+04
AF2 + OH → P10 + CH$_2$CHCHO		4.18E−15	0.64	2.64E+04
AF2 + OH → P11 + CO		1.58E−24	3.75	1.86E+04
AF2 + OH → P12 + CH$_3$CH$_2$CHO		1.38E−57	15.13	7.45E+03

the reaction R7, INT1 breaks the C−C bond via transition state TS6 to generate 2-furancarboxylic acid (P6) + CH$_3$ has an energy barrier of −4.4 kcal•mol^{-1}. In terms of energy, the energy barrier of reaction R7 is smaller than that of R6, so after the addition of OH to AF2 to form INT1, INT1 is mainly consumed through reaction R7.

The addition reaction of AF2 with OH produces INT2, which is followed by the consumption of INT2 by β-dissociation R9 and R10. In R9, INT2 generates 2-furanol (P7) and CH$_3$CO radicals by breaking the C−C bond and the transition state is TS9 which has an energy barrier of −1.9 kcal•mol^{-1}. In R10, INT2 is first generated by breaking the C−O bond to form INT3 with a transition state of TS10 with an energy barrier of −9.9 kcal•mol^{-1}, and INT3 is followed by an intramolecular H-transfer to form INT4 with a transition state of TS11 with an energy barrier of 6.3 kcal•mol^{-1}. Eventually, INT4 dissociates to generate pent-4-ene-2,3-dione

(P8) and HCO radicals with a transition state of TS12, which has an energy barrier of 2.3 kcal•mol^{-1}.

AF2 undergoes the addition reaction with the OH to form INT5, which is subsequently consumed by β-dissociation of R12 and R13. INT5 subsequently breaks the C−O bond to produce INT6, which has an energy barrier of 22.6 kcal•mol^{-1} through the transition state TS14. INT6 generates C$_2$H$_2$ and P9 by dissociation reaction, and the transition state is TS15 at an energy barrier of 16.5 kcal•mol^{-1}. In addition, INT6 may also be isomerized to produce INT7 with a transition state of TS16, which has an energy barrier of 15.9 kcal•mol^{-1}. INT7 is finally dissociated to produce P10 and acrylaldehyde (CH$_2$═CH−CHO) with a transition state of TS17 which has an energy barrier of 7.0 kcal•mol^{-1}. It is evident from the PES that although the addition of OH to the C (3) site on the AF2 ring via reaction R11 to produce INT5 is not high in energy, the subsequent decomposition path of INT5 has a high energy

barrier, resulting in an uncompetitive addition path to the C (3) site on the furan ring.

The formation of INT8 by the addition reaction of AF2 with OH, the INT8 is subsequently consumed by β-dissociation of R15. In the reaction R15, INT8 was first generated through the TS19 with an energy barrier of 21.9 kcal•mol^{-1}, breaking the C−O bond to form INT9, and INT9 was followed by the isomerization reaction to form INT10 with the transition state TS20 with an energy barrier of 17.4 kcal•mol^{-1}. The INT10 eventually dissociates to form CO and P11 through the TS21 with an energy barrier of −9.3 kcal•mol^{-1}. Similar to reaction R11, the addition of the OH to the C (4) site on the AF2 ring via R14 to generate INT8 is not high in energy, but the energy barrier for the subsequent decomposition path of INT8 is high, resulting in an uncompetitive addition path to the C (4) site on the furan ring. Therefore, it is energetically obvious that OH-addition to the C (3) and C (4) sites of AF2 is not the main addition channel.

AF2 reacts with the OH in an addition reaction to form INT11, which is subsequently consumed by β-dissociation of R17. INT11 generates INT12 by breaking the C−O bond, with a transition state of TS23 and an energy barrier of −13.0 kcal•mol^{-1}. INT12 is followed by INT13 through intra-molecular H-transfer, with a transition state of TS24 and an energy barrier of 2.1 kcal•mol^{-1}. INT13 eventually generates propionaldehyde (CH$_3$CH$_2$CHO) and P12 by breaking the C−C bond, and the transition state is TS25 with an energy barrier of 2.1 kcal•mol^{-1}. Therefore, it is known that the main reaction channels for the addition reaction of AF2 and OH are the C (2) and C (5) sites.

3.2. Rate Coefficients of AF2 + OH. To further clarify the contribution between different reaction channels on the PES of AF2 and OH, the rate constants of the relevant reactions were calculated. The rate constants for the pressure range of 0.01−100 atm and temperature range of 300−1500 K were solved and fitted to the extended Arrhenius expressions, as shown in Table 1.

The total rate constants for the OH addition and OH H-abstraction reactions of the AF2 and OH reaction system are plotted in Figure 4. It can be seen that the total rate constants for the 2-acetylfuran-hydroxyl system show a pressure dependence, with the rate constant increasing as the pressure increases.

The rate constants of the main reactions on the PESs of AF2 and OH at pressures of 0.01 and 100 atm are compared in Figure 5. It can be seen that the H-abstraction reaction (R1) of the CH$_3$ on the AF2 branched chain is the most important reaction channel. The reaction rate constants for the H-
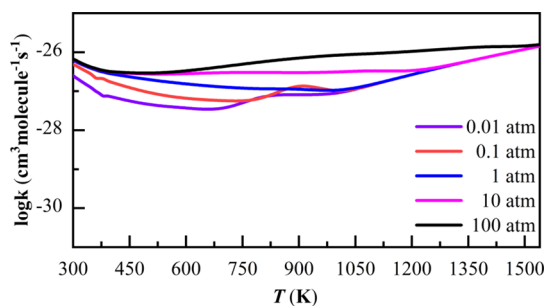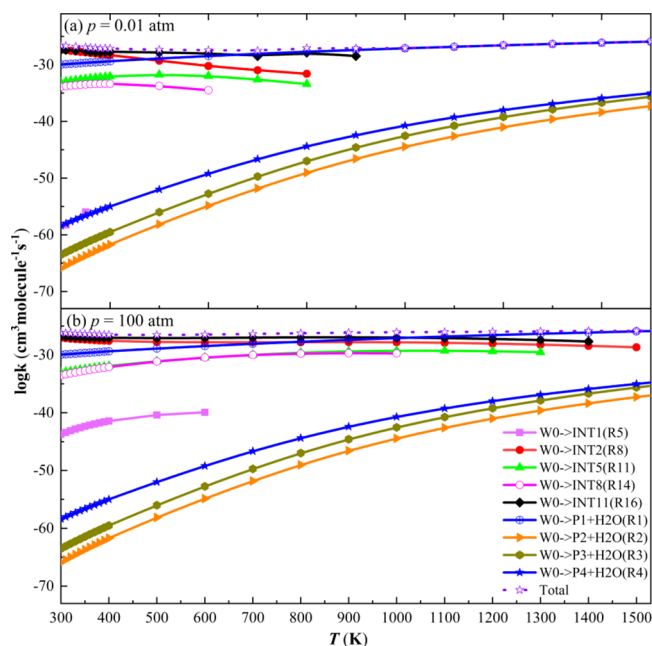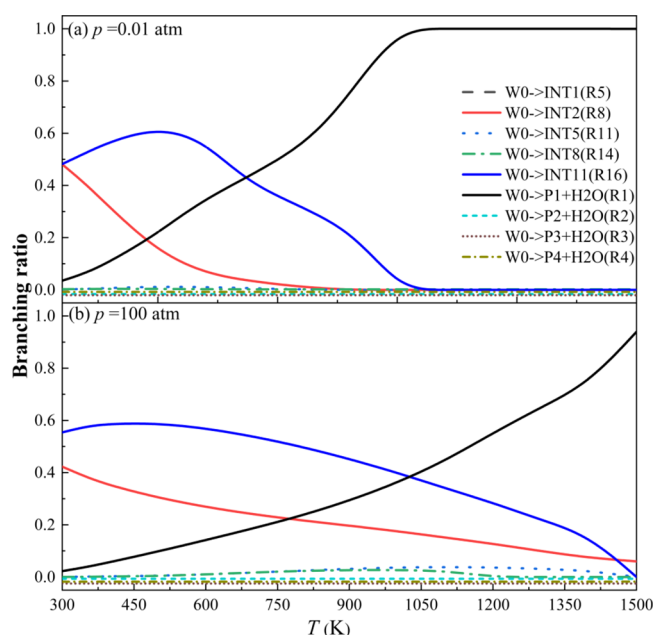

Figure 5. Rate constants for the reaction of AF2 with OH at pressures of 0.01 and 100 atm and temperatures ranging from 300 to 1500 K. (a) p = 0.01 atm; (b) p = 100 atm.

abstraction reactions (R2, R3, and R4) on the AF2 ring are several orders of magnitude lower than those for R1. As described in 3.1.1, the energy barrier required for the H-abstraction reactions on the AF2 ring is relatively high and therefore the H-abstraction reactions on the AF2 ring are unlikely to occur. It is interesting to note that the OH-addition reactions R8, R11, R14, and R16 on the AF2 ring are also the main reaction channels when the temperature is below 900 K. The range of rate coefficients for the OH-addition reaction becomes significantly larger as the pressure increases. However, the OH-addition reaction of the carbonyl group on the AF2 branched chain only contributes a little at low temperatures and is not competitive compared to the OH-addition reaction on the furan ring.

3.3. Branching Ratios of AF2 + OH. In order to further understand the AF2 + OH reaction system, the branching ratio of the reaction path on the PES, including five OH-addition reactions and four H-abstraction reactions was also calculated. The branching ratios of the rates of the nine reactions on the PES of the reaction of AF2 with OH at pressures of 0.01 and 100 atm and temperatures ranging from 300 to 1500 K are shown in Figure 6.

At 0.01 atm, the OH-addition reaction of C (2) and C (5) to produce INT2 and INT11 at temperatures of 300−500 K is the main reaction pathway (R8 and R16), and the branching ratio of these two pathways decreases from about 90% at 300 K to 0% at 1050 K as the temperature increases. The OH-addition reactions of the carbonyl group on the branched chain of AF2 and the OH-addition reactions of C (3) and C (4) on the furan ring produce INT1, INT3, and INT4, respectively, which have little effect on the consumption of AF2. In addition, the H-abstraction reaction (R1) of the CH$_3$ on the AF2 branched chain at 680−1500 K to produce P1 + H$_2$O is the most important channel for AF2 consumption. The percentage of R1 increases from 0.5% at 300 K to 100% at 1080 K with increasing temperature.

Figure 4. Total rate constants for OH-addition and OH H-abstraction reactions in the AF2 + OH reaction system.

Figure 6. Branching ratios of the reaction rate constants of AF2 and OH at pressures of 0.01 and 100 atm and temperatures ranging from 300 to 1500 K. (a) p = 0.01 atm; (b) p = 100 atm.

It can be seen from Figure 6 that at 100 atm is very similar to that at 0.01 atm, the H-abstraction reaction (R1) and the OH-addition reaction (R8 and R16) are still the three most competitive reaction pathways and there is no significant pressure dependence. However, the temperature range of the rate constants for R1, R8, and R16 is larger as the pressure increases. At 100 atm from 600 K, the OH-addition reactions of C (3) and C (4) on the furan ring produce INT5 and INT8, respectively, contributing only also less than 1% to the consumption of AF2.

As shown in Figure 6, at the current solved rate constants, the H-abstraction reaction on the branched CH_3 of AF2 is the most important depletion channel for AF2 in the higher temperature region. In contrast, in the lower temperature range, the OH-addition reactions (R8 and R16) on the AF2 rings C (2) and C (5) contribute significantly to the AF2 consumption, particularly at lower pressures.

4. CONCLUSIONS

In the current study, the PES of AF2 with OH was constructed using the CCSDT/CBS/M06-2x/cc-pVTZ method. Second, the temperature- and pressure-dependent rate constants for the relevant reactions in the PES of AF2 with OH were calculated by solving the master equation based on the transition state theory and Rice—Ramsperger—Kassel—Marcus theory, as well as Eckart tunneling effect correction. The calculations show that the OH forms a structure of a six-membered ring by weakly interacting hydrogen bonds with the carbonyl group and CH_3 on the AF2 branched chain, which is very stable and leads to a lower energy barrier, so that this reaction is the main H-abstraction pathway. The H-abstraction reaction on the AF2 ring does not occur easily due to the presence of a higher energy barrier. With regard to OH addition reactions, the addition reactions of the carbonyl group on the branched chain require higher energy barriers than those on C (2), C (3), C (4), and C (5) on the furan ring, and therefore the addition reactions of the carbonyl group on the branched chain are

unfavorable. The reaction system of AF2 and OH is dominated by the addition reactions at low temperatures, with the contribution of addition reactions decreasing as the temperature increases and the H-abstraction reactions on branched chains being the main reactions. In addition, the calculated reaction rate constants were fitted by the Arrhenius formula and given in the format in Chemkin software to provide theoretical support for future experimental and practical applications of the oxidation of AF2.

■ AUTHOR INFORMATION

Corresponding Authors

Liucun Zhu − *Advanced Science and Technology Research Institute, Beibu Gulf University, Qinzhou 535011, P.R. China; Research Institute for Integrated Science, Kanagawa University, Yokohama, Kanagawa 259-1293, Japan;* Email: lczhu@bbgu.edu.cn

Kang Shen − *Eastern Michigan Joint College of Engineering, Beibu Gulf University, Qinzhou 535011, P.R. China; Guangxi Key Laboratory of Ocean Engineering Equipment and Technology, Qinzhou 535011, P.R. China; College of Electrical Engineering, Guangxi University, Nanning, Guangxi 530004, P. R. China;* Email: shenkang945@bbgu.edu.cn

Authors

Wei He − *Eastern Michigan Joint College of Engineering, Beibu Gulf University, Qinzhou 535011, P.R. China; Guangxi Key Laboratory of Ocean Engineering Equipment and Technology, Qinzhou 535011, P.R. China; Education Department of Guangxi Zhuang Autonomous Region, Key Laboratory of Beibu Gulf Offshore Engineering Equipment and Technology (Beibu Gulf University), Qinzhou 535011, P.R. China;* ⊙ orcid.org/0000-0002-3100-9724

Kaixuan Chen − *Eastern Michigan Joint College of Engineering, Beibu Gulf University, Qinzhou 535011, P.R. China*

Complete contact information is available at:
https://pubs.acs.org/10.1021/acsomega.3c02636

Notes

The authors declare no competing financial interest.

■ REFERENCES

(1) Chen, Y. H.; Wang, C.; Nie, P. Y. Emission regulation of conventional energy-intensive industries. *Environ. Dev. Sustainability* **2020**, *22*, 3723−3737.

(2) Panahi, H. K. S.; Dehhaghi, M.; Kinder, J. E.; Ezeji, T. C. A review on green liquid fuels for the transportation sector: a prospect of microbial solutions to climate change. *Biofuel Res. J.* **2019**, *6*, 995−1024.

(3) Xie, H. L.; Yu, Y. N.; Wang, W.; Liu, Y. C. The substitutability of non-fossil energy, potential carbon emission reduction and energy shadow prices in China. *Energy Policy* **2017**, *107*, 63−71.

(4) York, R.; Bell, S. E. Energy transitions or additions? Why a transition from fossil fuels requires more than the growth of renewable energy. *Energy Res. Social Sci.* **2019**, *51*, 40−43.

(5) Bridgwater, A. V. Review of fast pyrolysis of biomass and product upgrading. *Biomass Bioenergy* **2012**, *38*, 68−94.

(6) Chu, S.; Majumdar, A. Opportunities and challenges for a sustainable energy future. *Nature* **2012**, *488*, 294−303.

(7) Bhutto, A. W.; Qureshi, K.; Abro, R.; Harijan, K.; Zhao, Z.; Bazmi, A. A.; Abbas, T.; Yu, G. R. Progress in the production of biomass-to-liquid biofuels to decarbonize the transport sector-prospects and challenges. *RSC Adv.* **2016**, *6*, 32140−32170.

(8) Diaz-Perez, M. A.; Serrano-Ruiz, J. C. Catalytic production of jet fuels from biomass. *Molecules* **2020**, *25*, 802.

(9) Roman-Leshkov, Y.; Barrett, C. J.; Liu, Z. Y.; Dumesic, J. A. Production of dimethylfuran for liquid fuels from biomass-derived carbohydrates. *Nature* **2007**, *447*, U982−U985.

(10) Zhao, H. B.; Holladay, J. E.; Brown, H.; Zhang, Z. C. Metal chlorides in ionic liquid solvents convert sugars to 5-hydroxymethylfurfural. *Science* **2007**, *316*, 1597−1600.

(11) Liu, X. F.; Yu, D. Y.; Luo, H. Y.; Li, C.; Li, H. Efficient reaction systems for lignocellulosic biomass conversion to furan derivatives: A minireview. *Polymer* **2022**, *14*, 3671.

(12) Khemthong, P.; Yimsukanan, C.; Narkkun, T.; Srifa, A.; Witoon, T.; Pongchaiphol, S.; Kiatphuengporn, S.; Faungnawakij, K. Advances in catalytic production of value-added biochemicals and biofuels via furfural platform derived lignocellulosic biomass. *Biomass Bioenergy* **2021**, *148*, No. 106033.

(13) Xu, N.; Gong, J.; Huang, Z. H. Review on the production methods and fundamental combustion characteristics of furan derivatives. *Renewable Sustainable Energy Rev.* **2016**, *54*, 1189−1211.

(14) Su, H. J.; Wang, J. L.; Zou, J. B.; Xu, Q.; Yang, J. Z.; Cheng, Z. J.; Wei, L. X. Experimental and kinetic modeling studies of 3-methylfuran pyrolysis at low and atmospheric pressures. *Energy Fuels* **2020**, *34*, 981−988.

(15) Whelan, C. A.; Eble, J.; Mir, Z. S.; Blitz, M. A.; Seakins, P. W.; Olzmann, M.; Stone, D. Kinetics of the reactions of hydroxyl radicals with furan and its alkylated derivatives 2-methyl furan and 2,5-dimethyl furan. *J. Phys. Chem. A* **2020**, *124*, 7416−7426.

(16) Wang, J. L.; He, S. R.; Wang, H.; Cheng, Z. J.; Wei, L. X.; Wang, J.; Yang, J. Z.; Yan, B. B.; Chen, G. Y. Experimental and kinetic modeling studies of the low-temperature oxidation of 2-methylfuran in a jet-stirred reactor. *Combust. Flame* **2021**, *233*, No. 111588.

(17) Jin, Z. H.; Yu, D.; Liu, Y. X.; Tian, Z. Y.; Richter, S.; Braun-Unkhoff, M.; Naumann, C.; Yang, J. Z. An experimental investigation of furfural oxidation and the development of a comprehensive combustion model. *Combust. Flame* **2021**, *226*, 200−210.

(18) Li, P.; He, W.; Wang, J.; Song, S.; Wang, J.; Lv, T.; Yang, J.; Cheng, Z.; Wei, L. Experimental and kinetic modeling investigations on low-temperature oxidation of 2-ethylfuran in a jet-stirred reactor. *Combust. Flame* **2022**, *241*, No. 112098.

(19) Zhang, L. D.; Chen, Q. X.; Zhang, P. A theoretical kinetics study of the reactions of methylbutanoate with hydrogen and hydroxyl radicals. *Proc. Combust. Inst.* **2015**, *35*, 481−489.

(20) Zhou, X. Y.; Zhai, Y. T.; Ye, L. L.; Zhang, L. D. Theoretical studies on the reaction kinetics of methyl crotonate with hydroxyl radical. *Sustainable Energy Fuels* **2018**, *2*, 392−402.

(21) Jin, H. F.; Liu, D. P.; Zou, J. B.; Hao, J. Y.; Shao, C.; Sarathy, S. M.; Farooq, A. Chemical kinetics of hydroxyl reactions with cyclopentadiene and indene. *Combust. Flame* **2020**, *217*, 48−56.

(22) He, W.; Lu, J.; Zhang, L. D.; Liu, J.; Wei, L. X. Theoretical studies on the reaction kinetics of methyl 2-furoate with hydroxyl radical. *Chin. J. Chem. Phys.* **2022**, *35*, 664−672.

(23) Xing, L.; Cui, J.; Lian, L.; Wang, J.; Wang, H.; He, Y.; Wang, S.; Wang, X.; Xu, L.; Cheng, Z. Ab initio kinetics of OH-initiated reactions of 2-furfuryl alcohol. *Fuel* **2023**, *338*, No. 127325.

(24) Zhao, Y.; Truhlar, D. G. The M06 suite of density functionals for main group thermochemistry, thermochemical kinetics, non-covalent interactions, excited states, and transition elements: two new functionals and systematic testing of four M06-class functionals and 12 other functionals. *Theor. Chem. Acc.* **2008**, *120*, 215−241.

(25) Frisch, G.W.T. M. J.; Schlegel, H. B.; Scuseria, G. E.; Robb, M. A.; Cheeseman, J. R.; Scalmani, G.; Barone, V.; Mennucci, B.; Petersson, G. A.; Nakatsuji, H.; Caricato, M.; Li, X.; Hratchian, H. P.; Izmaylov, A. F.; Bloino, G. Z. J.; Sonnenberg, J. L.; Hada, M.; Ehara, M.; Toyota, K.; Fukuda, R.; Hasegawa, J.; Ishida, M.; Nakajima, T.; Honda, Y.; Kitao, O.; Nakai, H.; Vreven, T.; Montgomery, J. J. A.; Peralta, J. E.; Ogliaro, F.; Bearpark, M.; Heyd, J. J.; Brothers, E.; Kudin, K. N.; Staroverov, V. N.; Keith, T.; Kobayashi, R.; Normand, J.; Raghavachari, K.; Rendell, A.; Burant, J. C.; Iyengar, S. S.; Tomasi, J.; Cossi, M.; Rega, N.; Millam, J. M.; Klene, M.; Knox, J. E.; Cross, J. B.; Bakken, V.; Adamo, C.; Jaramillo, J.; Gomperts, R.; Stratmann, R. E.; Yazyev, O.; Austin, A. J.; Cammi, R.; Pomelli, C.; Ochterski, J. W.; Martin, R. L.; Morokuma, K.; Zakrzewski, V. G.; Voth, G. A.; Salvador, P.; Dannenberg, J. J.; Dapprich, S.; Daniels, A. D.; Farkas, O.; Foresman, J. B.; Ortiz, J. V.; Cioslowski, J.; Fox, D. J. *Gaussian 09*; Gaussian Inc.: Wallingford CT, 2013.

(26) S.J.K. Y. Georgievskii, MESS.2016.3.23. Argonne National Laboratory, https://tcg.cse.anl.gov/papr/codes/mess.html, 10.1021/acs.jctc.1c00386.

(27) Georgievskii, Y.; Miller, J. A.; Burke, M. P.; Klippenstein, S. J. Reformulation and solution of the master equation for multiple-well chemical reactions. *J. Phys. Chem. A* **2013**, *117*, 12146−12154.

(28) Hippler, H.; Troe, J.; Wendelken, H. J. Collisional deactivation of vibrationally highly excited polyatomic-molecules 2 direct observations for excited toluene. *J. Chem. Phys.* **1983**, *78*, 6709−6717.

(29) Joback, K. G.; Reid, R. C. Estimation of pure-component properties from group-contributions. *Chem. Eng. Commun.* **1987**, *57*, 233−243.

(30) He, W.; Xu, Q.; Xie, C.; Yin, J.; Li, P.; Wang, Z.; Zhang, L.; Wei, L. Experimental and kinetic modeling studies of 2-acetylfuran pyrolysis at atmospheric pressure. *Combust. Flame* **2022**, *236*, No. 111824.